Optical properties of InGaAs/InAlAs diffused double quantum wells

Wallace C. H. Choy[a)]
National Research Council of Canada, Institute for Microstructural Sciences, M23A, Montreal Road, Ottawa K1A 0R6, Canada

(Received 14 May 1999; accepted for publication 4 December 1999)

The effects of interdiffusion on the subbands and optical properties of InGaAs/InAlAs double quantum well (QW) have been theoretically studied. The results show that since a double QW (DQW) can be diffused to become an effectively single QW structure, the characteristic features in the subbands structure and optical properties of a strongly coupled DQW structure and that of a single QW structure can be obtained by a suitable annealing time. Moreover, the increase in separation between the first symmetric and antisymmetric heavy hole subbands and the increase in the spin splitting of the valence subbands of the diffused DQW, due to an applied electric field, diminish when annealing time increases. In optimizing the $In_{0.53}(Al_aGa_{1-a})_{0.47}As/In_{0.52}Al_{0.48}As$ DQW structure, the results show that symmetric DQW with no Al content in wells can provide large material gain and radiative spontaneous recombination rate. With interdiffusion, the material gain and recombination rate reduce but the reduction saturates when the DQW structure is diffused to effectively become a single graded QW. By subjecting the DQW and an as-grown single QW to the same annealing conditions (where the summation of the width of the two wells and the separation barrier of the DQW equals the well width of the single QW), the diffused DQW can provide a larger material gain and radiative recombination rate than the diffused single QW when the annealing time is short. Therefore, the short-time diffused DQW is more useful for laser applications. Besides, since Al diffuses into the wells, the transition energy of the QW structure increases so that the operating wavelength of the optical devices can be adjusted. © *2000 American Institute of Physics.* [S0021-8979(00)02706-7]

I. INTRODUCTION

Different methods of interdiffusion in InGaAs/InAlAs quantum wells (QWs) have been investigated recently. They include dopant-induced interdiffusion technology using, for example, Si[1,2] and dopant free interdiffusion technology using SiO_2 capping,[3,4] Si_3N_4 capping,[5] and bare QW interdiffusion.[6] After a rapid thermal annealing, all these interdiffusion technologies result in an increase in the transition energy of the QW structure. The blueshift of the transition energy can be enhanced using a repetitive rapid thermal annealing as compared to a single-slot annealing with an amount of time equal to the total annealing time of the repetitive one.[5] Besides, the reported results[1,6] have been obtained for bare interdiffusion showing that the transition energy can be slightly blueshifted with less than 5 meV measured at room temperature using 60 min of 700 °C thermal annealing[1] and substantially blueshifted with more than 20 meV measured at 77 K after 5 s of lamp annealing.[6] For optical device applications, the SiO_2 capped QW interdiffusion technology may be the better candidate[3,4] because of the following: (a) it can enhance the interdiffusion as compared to the bare QW interdiffusion, (b) the broadening of the PL spectrum can be improved as compared to the Si doped one, and (c) the PL efficiency of the diffused QW with SiO_2 capping can be considerably enhanced by a factor of up to 26, depending on the QW structure and the diffusion conditions,[4] i.e., the quality of the QW may be improved and thus could be beneficial for optical devices. Consequently, with appropriate interdiffusion, the operating wavelength of a InGaAs/InAlAs QW optical device can be adjusted and the optical properties, i.e., the performance, of the optical device can be improved.

Currently, coupling effects in double quantum wells (DQWs) for use in optical devices have been of considerable interest. By optimizing the DQW structure, the coupling effects can provide a large blueshift of the transition energy,[7] a large refractive index change,[8] an enhanced absorption change,[9] or a strong gain switching[10] as with the quantum confined Stark effect. However, for the InGaAs/InAlAs DQW structure, there are only a few reports on its optical properties[11] and the modeling has not taken into account the band mixing effect of valence subbands and the coupling effect of excitons, which will have significant effects on the QW optical properties. Moreover, to our knowledge, there is no report on the effects of interdiffusion on the DQW structure.

In this article, $In_{0.53}Ga_{0.47}As/In_{0.52}Al_{0.48}As$ diffused DQW are investigated theoretically, taking into account the strain effects induced by interdiffusion, carrier effects, the band-mixing effects of valence subbands, and coupling of excitons. The effects of interdiffusion on the subband structure and optical properties of DQW are discussed. With the consideration of the saturation of excitonic absorption, the changes of absorption, gain, and refractive index due to applied electric fields are addressed.

a)Author to whom correspondence should be addressed. Electronic mail: wallace.choy@nrc.ca

II. MODELING

For a InGaAs/InAlAs QW structure, interdiffusion involving the three group III atoms; In, Ga, and Al, can be described by coupled equations expanded from Fick's second law:[12]

$$\frac{\partial C_1}{\partial t}=\frac{\partial}{\partial x}\left(D_{11}\frac{\partial C_1}{\partial x}\right)+\frac{\partial}{\partial x}\left(D_{12}\frac{\partial C_2}{\partial x}\right), \tag{1}$$

$$\frac{\partial C_2}{\partial t}=\frac{\partial}{\partial x}\left(D_{21}\frac{\partial C_1}{\partial x}\right)+\frac{\partial}{\partial x}\left(D_{22}\frac{\partial C_2}{\partial x}\right), \tag{2}$$

where C_1 and C_2 denote In and Ga, respectively. D_{11} and D_{22} are the cross-diffusion rates of In–In and Ga–Ga, respectively, and D_{12} and D_{21} are the cross-diffusion rates of In–Ga and Ga–In, respectively. The diffusion terms incorporating D_{12} and D_{21} indicate that the interdiffusion of In and Ga are mutually interactive. From the stoichiometry boundary condition, the Al concentration profile can be obtained using $1-C_1-C_2$. Consequently, a quaternary $In_xAl_yGa_{1-x-y}As$ material system will form in the QW structure after interdiffusion.

In modeling the subband structure, the coupling of the heavy hole (HH) and light hole (LH) is considered using the 4×4 Luttinger–Kohn Hamiltonian.[13] The Hamiltonian for the valence band of a diffused DQW can be written as

$$\begin{pmatrix} P+Q+V_{\mathrm{HH}}(z) & \Omega & -B & 0 \\ \Omega^* & P-Q+V_{\mathrm{LH}}(z) & 0 & B \\ -B^* & 0 & P-Q+V_{\mathrm{LH}}(z) & \Omega \\ 0 & B^* & \Omega^* & P+Q+V_{\mathrm{HH}}(z) \end{pmatrix}, \tag{3}$$

where

$$P=\frac{\hbar^2}{2m_0}\gamma_1(z)(k_x^2+k_y^2+k_z^2),$$

$$Q=\frac{\hbar^2}{2m_0}\gamma_2(z)(k_x^2+k_y^2-2k_z^2),$$

$$V_{\mathrm{HH}}(z)=\tilde{V}^V(z)-|e|Fz+|e|\varphi(z)-(1-Q_c)S_\perp(z)+S_{\parallel\mathrm{HH}}(z),$$

$$V_{\mathrm{LH}}(z)=\tilde{V}^V(z)-|e|Fz+|e|\varphi(z)-(1-Q_c)S_\perp(z)+S_{\parallel\mathrm{LH}}(z),$$

$$\Omega=-\frac{\hbar^2}{m_0}\left(\frac{\sqrt{3}}{2}\overline{\gamma}(z)(k_x-ik_y)^2-\frac{\sqrt{3}}{4}[\gamma_3(z)-\gamma_2(z)]\times(k_x+ik_y)^2\right),$$

$$B=\sqrt{3}\frac{\hbar^2}{m_0}\gamma_3(z)k_z(k_x-ik_y),$$

where z denotes the growth direction, $\tilde{V}^V(z)$ is the diffused potential profile of the valence band, and F and $\varphi(z)$ are the applied electric field and the potential due to carriers, respectively. Q_c is the conduction band offset ratio and the well center is defined as being at $z=0$. $S_\perp$, $S_{\parallel\mathrm{HH}}$ and $S_{\parallel\mathrm{LH}}$ are the biaxial component of strain, and the splitting energy of HH and LH induced by the uniaxial component of the strain respectively. The detailed relationships have been discussed previously.[14] m_0 is an electron mass, $\gamma_1(z)$, $\gamma_2(z)$, and $\gamma_3(z)$ are the Luttinger–Kohn parameters,[15] $\overline{\gamma}(z)=1/2[\gamma_2(z)+\gamma_3(z)]$, and $k_\parallel=k_x\hat{x}+k_y\hat{y}$. The fourfold degenerate envelope functions that satisfy Eq. (3) have quantum numbers' $-3/2$, $-1/2$, and $3/2$ (HH$=\pm3/2$, LH$=\pm1/2$). For simplicity, the axial approximation, which assumes that $\gamma_2(z)=\gamma_3(z)$, is applied to the Ω term and the 4×4 Hamiltonian is transformed into two 2×2 Hamiltonians H^U and H^L:[16,17]

$$H^\sigma=\begin{bmatrix} P\pm Q+V_{\mathrm{HH}}(z) & \xi \\ \xi^* & P\mp Q+V_{\mathrm{LH}}(z) \end{bmatrix}, \tag{4}$$

where the superscript $\sigma=U$ or L and $\xi=\Omega+i|B|$. The new basis consisting of eigenstates $|1\rangle$, $|2\rangle$, $|3\rangle$, and $|4\rangle$ for H^U and H^L are formed from the original basis with quantum numbers $-3/2$, $-1/2$, $1/2$, and $3/2$. To solve Hermitian Hamiltonian H^U and H^L, the effective mass approximation has been used such that $k_z=-i(\partial/\partial z)$. The eigenvalue equations have been solved using the finite different method.

The conduction band at the Γ valley ($k_\parallel=0$) is modeled using the one-dimensional one particle Schrödinger-like equation obtained from an envelope function approximation:[18,19]

$$\frac{-\hbar^2}{2}\frac{d}{dz}\left[\frac{1}{m_e^*(z)}\frac{d}{dz}+\tilde{V}^C(z)+|e|Fz-|e|\varphi(z)-Q_cS_\perp(z)\right]\psi_a^C(z)=E_a^C\psi_a^C(z), \tag{5}$$

where $\tilde{V}^C(z)$ is the diffused potential profile of the conduction band, $m_e^*(z)$ is the effective mass of an electron, and $\psi_a^C(z)$ represents the envelope function of the ath electron confined state with energy E_a^C.

The potential $\varphi(z)$ which contributes to the free-carrier screening effects can be obtained by solving Poisson's equation (6) self-consistently with Eqs. (4) and (5)

$$\frac{d^2}{dz^2}\varphi(z)=-\frac{|e|}{\varepsilon}[p(z)-n(z)+N_D(z)-N_A(z)], \tag{6}$$

where ε is the dielectric constant of the well, and N_D and N_A are the density of the ionized donors and acceptors, respectively. For simplification, N_D and N_A are assumed to be zero. The carrier densities $p(z)$ and $n(z)$ are given as

$$p(z)=\frac{1}{2\pi}\int_{k_\parallel}\sum_{\sigma}\sum_{b}|\Psi^{V\sigma}_{bk_\parallel}(r)|^2[1-f^{V\sigma}_b(k_\parallel)]k_\parallel\,dk_\parallel, \tag{7}$$

$$n(z)=\frac{m_e k_B T}{\pi\hbar^2}\sum_{a}|\psi^C_a(z)|^2\ln\left[1+\exp\left(\frac{F_n-(E^C_a-E^C_1)}{k_BT}\right)\right], \tag{8}$$

where k_B and T are the Boltzmann constant and temperature, respectively, and F_n is the quasi-Fermi level for the electron in the conduction band. $f^{V\sigma}_b(k_\parallel)$ and $\Psi^{V\sigma}_{bk_\parallel}$ are the electron Fermi distribution function and the envelope function for the bth subband in the valence band of H^σ, respectively. $p(z)$ is determined with the consideration of the band mixing effects of the valence band, while $n(z)$ is calculated by assuming that the conduction band dispersion is parabolic.

When the energy difference between the first and second subband states is small such as in DQW, the intersubband coupling of the excitons has to be considered. The variational wave function $\chi(\rho)$ associated with the lowest two subband states of the electron and the hole are chosen as[20]

$$\chi(\rho)=\sum_{a=1}^{N}\sum_{b=1}^{M}d_a\psi^C_a(z)f_b\phi^V_b(z)e^{-\beta\rho}, \tag{9}$$

where ϕ^V_b is the $k_\parallel=0$ envelope function of the bth subband in the valence band of H^U, N and M are the number of the electron and hole states in calculation, both having a value of 2, and ρ is the displacement of the two position vectors $\mathbf{r}_e$ and $\mathbf{r}_h$ projected in the x-y plane. β is a variational parameter governing the radial extent of the wave function and d_a and f_b are variational parameters which are subject to the normalization constraints

$$\sum_{a=1}^{N}|d_a|^2=1,\quad \sum_{b=1}^{M}|f_b|^2=1. \tag{10}$$

The minimized expectation value of the exciton Hamiltonian $E_{\rm exc}$, which is the total exciton energy, can be determined by

$$E_{\rm exc}=\langle\chi|H_{\rm exc}|\chi\rangle/\langle\chi|\chi\rangle. \tag{11}$$

The exciton binding energy E_b is then obtained

$$E_b=E^C+E^V-E_{\rm exc}, \tag{12}$$

where E^C and E^V are the electron and hole state energy, respectively.

With the subband structure, the material gain with a spectral broadening at transition energy E is modeled using the density of state approach

$$g(E)=\int dE\sum_{\sigma}\sum_{a,b}\frac{q^2\hbar}{2\pi n_R\varepsilon_0 c m_0^2 L_z E}\int d^2k_\parallel|\hat{e}\cdot\mathbf{P}^\sigma_{ab}(k_\parallel)|^2 \cdot\delta[E^C_a(k_\parallel)-E^V_{\sigma b}(k_\parallel)+E_g-E] \times[f^C((E^C_a k_\parallel))-f^{V\sigma}_b(k_\parallel)]L(E'-E), \tag{13}$$

where $\sigma=U$ or L. c, n_R, and q are the speed of light, refractive index, and electric charge, respectively. L_z is the total thickness of two wells and the separation barrier of the as-growth DQW, E_g is the band gap energy, and E' is the photon energy, $E^{V\sigma}_b$ is the bth subband energy in the valence band of H^σ, and $L(E'-E)$ is the Lorentzian line-broadening function. $\mathbf{P}^\sigma_{ab}$ is the optical matrix element for the transition between the ath conduction subband and the bth valence subband, $\hat{e}$ is a unit vector along the polarization direction of the optical electric field. $f^C(E^C_a)$ is the electron Fermi distribution function of the ath conduction subband. The squared optical matrix elements $|\hat{e}\cdot\mathbf{P}^\sigma_{ab}|^2$ are, for TE mode polarization

$$\begin{aligned}|\hat{e}\cdot\mathbf{P}^U_{ab}(k_\parallel)|^2&=|\langle x|P|s\rangle|^2\cdot[\tfrac{1}{2}|\langle\psi^C_a|\psi^V_{1b}\rangle|^2\\&\quad+\tfrac{1}{6}|\langle\psi^C_a|\psi^V_{2b}\rangle|^2],\\|\hat{e}\cdot\mathbf{P}^L_{ab}(k_\parallel)|^2&=|\langle x|P|s\rangle|^2\cdot[\tfrac{1}{2}|\langle\psi^C_a|\psi^V_{4b}\rangle|^2\\&\quad+\tfrac{1}{6}\langle\psi^C_a|\psi^V_{3b}|^2\rangle],\end{aligned} \tag{14}$$

where ψ^V_{ib} is the z direction envelop function for the bth subband in the valence band of H^σ and the subscript i denotes the ith eigenstate of the new basis. In determining the momentum matrix elements $\langle x|P|s\rangle$, the expression

$$|\langle x|P_x|s\rangle|^2=\frac{m_0^2}{2m_e^*}\frac{E_g(E_g+\Delta)}{E_g+\frac{2}{3}\Delta} \tag{15}$$

is used where Δ is the spin-orbit splitting energy.

The rate of the radiative spontaneous recombination τ can be determined as

$$\tau(E)=\int dE\sum_{\sigma}\sum_{a,b}\frac{q^2\hbar}{2\pi n_R\varepsilon_0 m_0^2 L_z E}\int d^2k_\parallel|\hat{e}\cdot\mathbf{P}^\sigma_{ab}(k_\parallel)|^2\cdot\delta[E^C_a(k_\parallel)-E^V_{ab}(k_\parallel)+E_g-E] \times[f^C(E^C_a(k_\parallel))-f^{V\sigma}_b(k_\parallel)+1]L(E'-E). \tag{16}$$

The bound state absorption coefficient $\alpha_{\rm bd}(E)$ can be obtained by

$$\alpha_{\rm bd}(E)=-G(E) \tag{17}$$

and the exciton absorption coefficient $\alpha^0_{\rm exc}(E)$ is determined using[8,21]

$$\alpha^0_{\rm exc}(E)=\frac{e^2\hbar E}{2cn_R\varepsilon_0 m_e^* E_{CV}^2 L_z}\left(\frac{E_g(E_g+\Delta_0)}{E_g+2/3\Delta_0}\right)\times\frac{\frac{2\beta^2}{\pi}|\psi(\rho)|^2\wp\Gamma_{XB}}{\pi[(E_{\rm exc}-E)^2+\Gamma^2_{XB}]}, \tag{18}$$

where Γ_{XB} is the exciton linewidth (half-width at half-maximum) broadening factor, $\wp$ is the polarization factor,

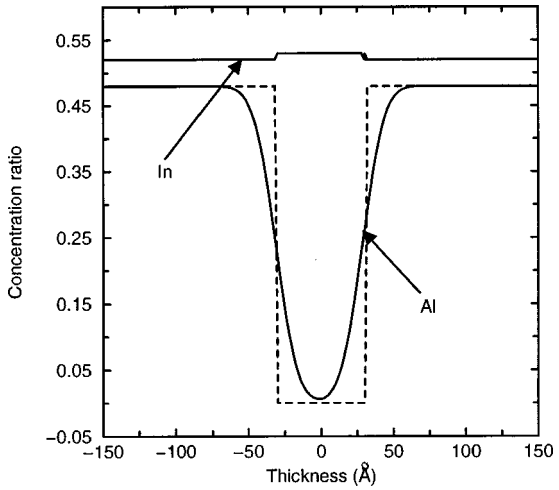

FIG. 1. In and Al concentration profiles of $In_{0.53}Ga_{0.47}As/In_{0.52}Al_{0.48}As$ diffused single QW with $L_z=60$ Å; annealing time $t=0$ (dashed line), and $t=18$ s (solid line).

and E_{CV} is the transition energy between a conduction subband and a valence subband at $k_{\|}=0$. The saturation of exciton absorption can be considered by assuming that the exciton, electrons, and holes are in thermodynamic equilibrium.[22] The exciton absorption coefficient α_{exc} with saturation effects can be written as

$$\alpha_{\text{exc}}=\alpha_{\text{exc}}^{0}(1-N_{\text{exc}}A_{\text{exc}})\exp[-(N_e+N_h)A_{\text{exc}}], \tag{19}$$

where N_{exc} and A_{exc} are the two-dimensional (2D) exciton density and area of one exciton, respectively. N_{exc} can be obtained using

$$\frac{N_eN_h}{N_{\text{exc}}}=\frac{m_e^*}{\pi\hbar^2}(k_BT)\exp\left(-\frac{E_b}{k_BT}\right). \tag{20}$$

The total absorption coefficient α_{tot} equals $\alpha_{\text{bd}}+\alpha_{\text{exc}}$. The change of α_{tot} due to the injected carriers will vary the refractive index and the change of refractive index is determined using Kramer–Krönig transformation. It should be noted that many body effects of free carriers will modify the excitonic features, although it has not been considered in this article.

III. RESULTS AND DISCUSSIONS

The effects of interdiffusion on the $In_{0.53}Ga_{0.47}As/In_{0.52}Al_{0.48}As$ DQW subband structures and optical properties are first discussed. With an understanding of the diffused DQW, the effects of injected carriers and applied electric fields are addressed. The structure of the DQW studied in this article has two identical wells with thickness of 50 Å separated by a thin barrier with thickness of 20 Å, except for the section of optimizing the $In_{0.53}(Al_aGa_{1-a})_{0.47}As/In_{0.52}Al_{0.48}As$ DQW structure. $p(z)$ is considered to be equal to $n(z)$ and Q_c is taken as 0.72.[23] In calculating the optical properties, the full-width-half-maximum exciton and bound state broadening factors are considered to be the same and both have a value of 10 meV. Due to the Pauli exclusion principle, a sublevel in a single QW will split into two: symmetric and antisymmetric states

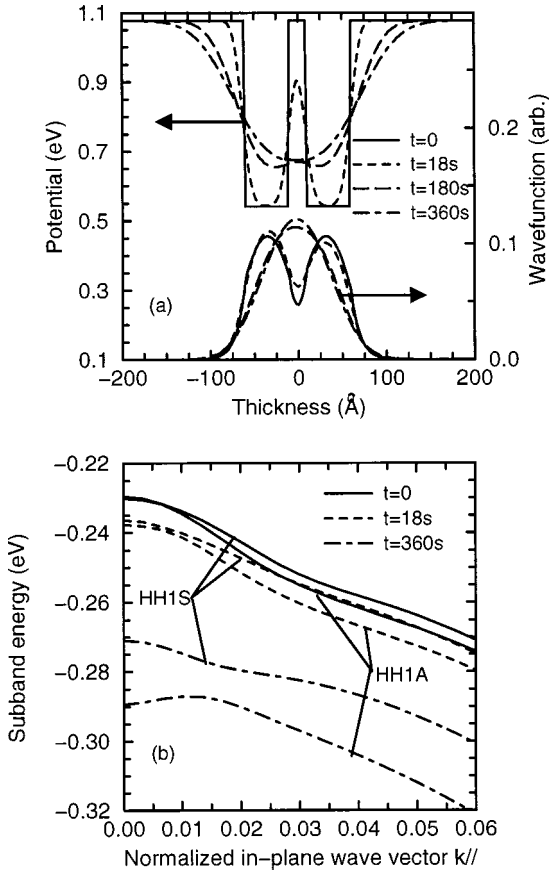

FIG. 2. (a) The conduction-band potential profile and $C1S$ envelope function of $In_{0.53}Ga_{0.47}As/In_{0.52}Al_{0.48}As$ diffused DQW with two 50 Å wells and separated by a 20 Å barrier; $t=0$ (solid line), $t=18$ s (dashed line), $t=180$ s (long-dashed line), and $t=360$ s (dashed–dotted line), (b) HH1S and HH1A subband structures; $t=0$ (solid line), $t=18$ s (dashed line), and $t=360$ s (dashed–dotted line). The in-plane wave vector $k_{\|}$ is normalized with $2\pi/a_0$, where a_0 is a lattice constant.

in DQW. The first symmetric and antisymmetric states of HH are denoted by HH1S and HH1A, respectively. Similarly for that of other bands such as LH, the states are denoted by LH1S and LH1A.

A. Effects of interdiffusion

For the interdiffusion of the three species In, Ga, and Al, the cross-diffusion coefficients of long-time diffused InGaAs/InAlAs QW annealed for 10 h at 1085 K and short-time diffused QW annealed for 15 s at 1173 K have been reported.[2,4,12] In this article, since all studied QW structures are considered to be annealed at a short annealing time ($\leqslant$360 s), the cross-diffusion coefficients of the short time diffused QW annealed at 1173 K (Ref. 4) have been used here. They include $D_{\text{In–In}}=D_{\text{In–Ga}}=D_{\text{Ga–In}}=0$ and $D_{\text{Ga–Ga}}=2\times10^{-16}\,\text{cm}^2\,\text{s}^{-1}$. After an annealing time of $t=18$ s, the diffused Al profile becomes graded as compared with the as-grown one and the In profile in a $In_{0.53}Ga_{0.47}As/In_{0.52}Al_{0.48}As$ single QW with a well width of 60 Å remains abrupt, as in Fig. 1. In addition, the $C1-HH1$ energy increases from 0.8606 to 0.8947 eV after annealing. The effective interdiffusion is an isotropic Al and Ga interdiffusion. This equalized mobility of Al and Ga sublattices

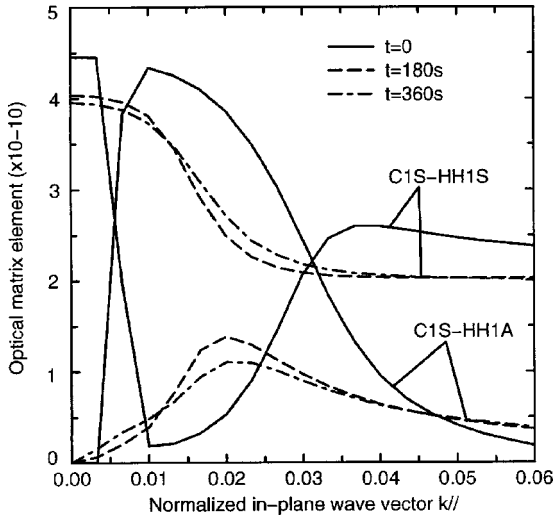

FIG. 3. TE optical matrix elements of $C1S-\mathrm{HH1}S$ and $C1S-\mathrm{HH1}A$ for the H^L valence band of the diffused DQW; $t=0$ (solid line), $t=180$ s (long-dashed line), and $t=360$ s (dashed–dotted line).

without any significant modification of the In profile may be explained by the transient effects[2] which occur when the annealing time is short ($t<1$ h).

For the $In_{0.53}Ga_{0.47}As/In_{0.52}Al_{0.48}As$ DQW, when t increases, the potential profile becomes graded and the thin separation barrier becomes lower and broader. When $t \geqslant 180$ s, the two wells of the DQW potential profile combine to become a single graded well, as in Fig. 2(a). At the same time, the two peaks of the envelope function merge to become a single peak at the center of the well. Before any interdiffusion, the HH1S and HH1A subbands are close to each other when $k_{\|}\rightarrow 0$ as shown in Fig. 2(b). However, when t increases, the HH1S and HH1A subbands move away from each other. At $t=360$ s, since a single graded well potential forms, HH1S and HH1A physically behave as HH1 and HH2, respectively. Generally, since more Al diffuses into the wells with increasing t, valence subbands move down and transition energies increase. With regard to the optical matrix elements of diffused DQWs, when $t=0$, i.e., the as-grown DQW, the optical matrix elements of $C1S-\mathrm{HH1}S$ and $C1S-\mathrm{HH1}A$ at $k_{\|}=0$ are at their maximum and minimum, respectively, as in Fig. 3, because the overlapping integral of the $C1S$ envelope function with the HH1S and HH1A envelope function is at its highest and lowest values ($\sim$0.972 and $\sim$0.001), respectively. The two optical matrix elements change vigorously and rapidly in a short range of $k_{\|}$ from 0 to 0.01. However, when $t\geqslant 180$ s, the changes in the two optical matrix elements are more gradual along $k_{\|}$ because the DQW is diffused to approximately become a single graded QW, as in Fig. 2(a).

With interdiffusion, the gain peak of the DQW with an injected carrier density (n) of $5\times 10^{12}\,\mathrm{cm}^{-2}$ gradually decreases, as in Fig. 4(a). When $t\geqslant 180$ s, the reduction in the gain peak saturates. The variations of the gain peak cannot be explained by that of the electron and hole quasi-Fermi levels of the DQW due to interdiffusion, as in Fig. 5. It should be noted that the quasi-Fermi level is determined with respect to the lowest subband edge of the carrier and the

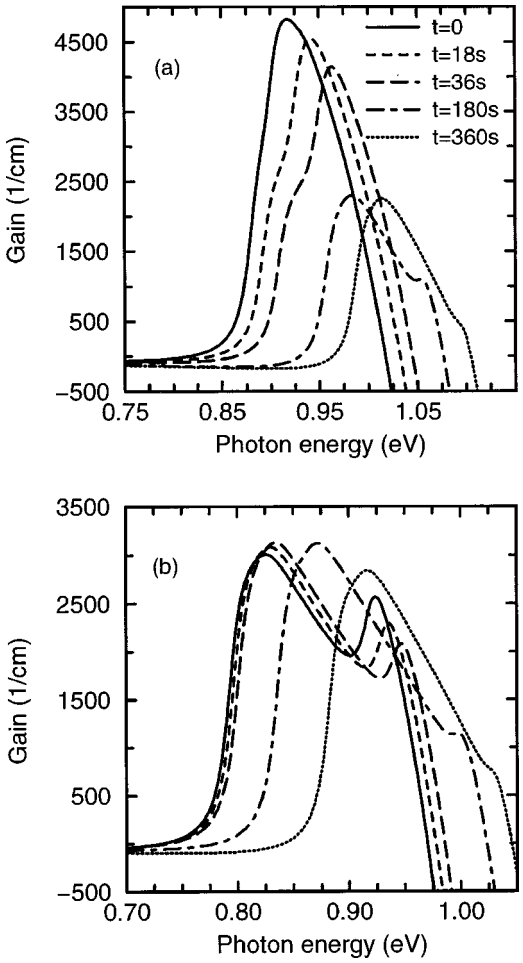

FIG. 4. TE gain spectra of: (a) $In_{0.53}Ga_{0.47}As/In_{0.52}Al_{0.48}As$ diffused DQW with $n=5\times 10^{12}\,\mathrm{cm}^{-2}$ and (b) $In_{0.53}Ga_{0.47}As/In_{0.52}Al_{0.48}As$ diffused single QW with $L_z=120$ Å and same carrier density as the DQW; $t=0$ (solid line), $t=18$ s (dashed line), $t=36$ s (long-dashed line), $t=180$ s (dashed–dotted line), and $t=360$ s (dotted line).

subband edge will change with interdiffusion. The increase of the electron and hole quasi-Fermi levels when $t\leqslant 36$ s and $t>180$ s, respectively, will increase material gain. However, the gain peak generally reduces when t increases as shown in Fig. 4(a). For the as-grown DQW, the transition energies of $C1S-\mathrm{HH1}S$ and $C1A-\mathrm{HH1}A$ are so close to each other with only 20 meV difference that the $C1S-\mathrm{HH1}S$ and $C1A-\mathrm{HH1}A$ gain peaks merge to become the single peak at 0.91 eV with the highest gain. However, when t increases, the difference between the two transition energies increases. At $t=360$ s, the difference is 110 meV so that the $C1A-\mathrm{HH1}A$ gain peak position is at the dip of the gain spectrum contributed to by the $C1S-\mathrm{HH1}S$ transition, which results in a two-peak gain spectrum and a reduction of gain-peak value. At the same time, the optical matrix elements decrease when $k_{\|}\rightarrow 0$, as in Fig. 3, which will decrease the material gain. Similar changes of the gain peak can also be obtained when the carrier population of diffused DQWs is fully inverted, i.e., the difference of Fermi function equals unity, as in Fig. 6. This implies that variations of the gain peak (decrease at $t\leqslant 180$ s and saturate at a longer t) are not directly contributed to by the variation of the quasi-Fermi

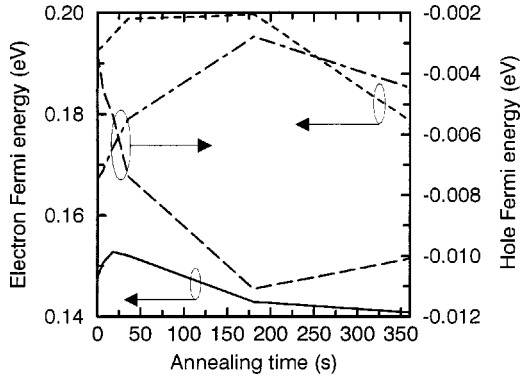

FIG. 5. Electron and hole quasi-Fermi-level energies $In_{0.53}Ga_{0.47}As/In_{0.52}Al_{0.48}As$ diffused DQW with $n=5\times10^{12}\,cm^{-2}$ and $In_{0.53}Ga_{0.47}As/In_{0.52}Al_{0.48}As$ diffused single QW with $L_z=120$ Å and same carrier density as the DQW; electron Fermi level of DQW (solid line), hole Fermi level of DQW (long-dashed line), electron Fermi level of single QW (dashed line), and hole Fermi level of single QW (dotted–dashed line).

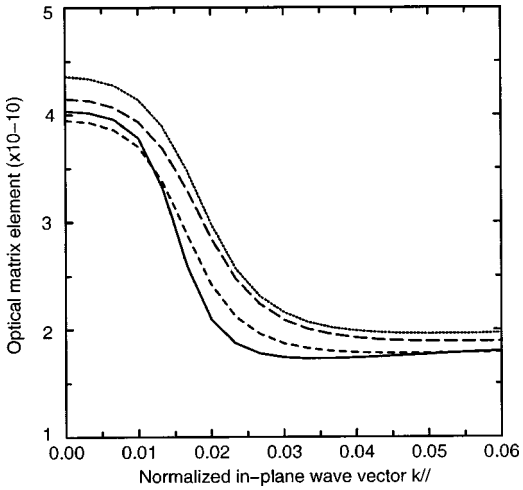

FIG. 7. The optical matrix element of the transition with the lowest photon energy for the valence band of H^U of the diffused DQW and the corresponding diffused single QW when the carrier population is fully inverted. Diffused DQWs with $t=180$ and 360 s are denoted by the solid line and dashed line, respectively. Diffused single QWs with $t=180$ and 360 s are denoted by the dotted line and long-dashed line, respectively.

levels due to interdiffusion. Consequently, when t increases: (a) the gain spectrum decreases primarily due to the increase in separation between $C1S-H1S$ and $C1A-H1A$, (b) the two separate peaks of the gain spectrum become more distinct.

Considering $In_{0.53}Ga_{0.47}As/In_{0.52}Al_{0.48}As$ single QW with $L_z=120$ Å and $n=5\times10^{12}\,cm^{-2}$, the gain peak increases when t increases from 0 to 180 s and then decreases for further interdiffusion, as in Fig. 4(b). This can be explained by the similar variations with interdiffusion exhibited by the quasi-Fermi levels, as in Fig. 5. Both electron and hole quasi-Fermi levels increase when $t\leqslant180$ s so that the material gain increases. However, for a longer t, quasi-Fermi levels decrease, which result in the reduction of material gain. Comparing the diffused DQW with $t=18$ s and the single QW annealed for the same amount of time, the gain peak of the diffused DQW is higher than that of the diffused single QW in the cases of $n=5\times10^{12}\,cm^{-2}$ and the fully inverted carrier population as shown in Figs. 4(b) and 6, respectively. The explanation for this is similar to that previously used for the gain reduction of diffused DQW due to the separation between $C1S-HH1S$ and $C1A-HH1A$ increased with interdiffusion. Here for the diffused DQW, the energy difference between the $C1S-HH1S$ and $C1A-HH1A$ transitions is only 33 meV, while that for the $C1-HH1$ and $C2-HH2$ transitions in the diffused single QW is 133 meV. As a result, the material gain of the diffused DQW is larger than that of the corresponding diffused single QW when $t<180$ s.

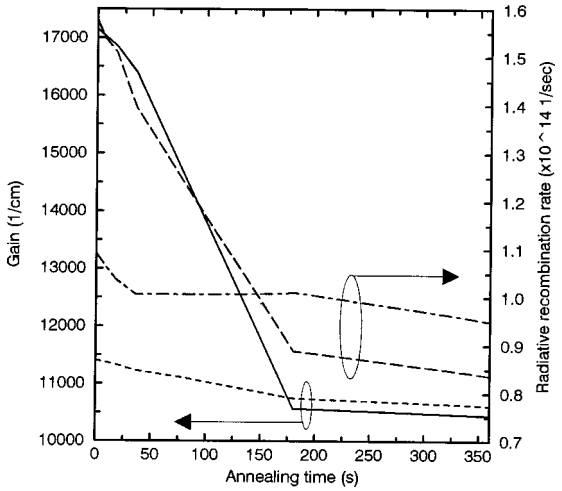

FIG. 6. The gain peak with the lowest photon energy and maximum τ of the diffused 50 Å/20 Å/50 Å DQW and the corresponding diffused single QW with $L_z=120$ Å. The gain peak is obtained when the carrier population is fully inverted and τ is determined when $n=5\times10^{12}\,cm^{-2}$; gain peak of DQW (solid line), gain peak of single QW (dashed line), τ of DQW (long-dashed line), and τ of single QW (dashed–dotted line).

Interestingly, the gain-peak spectra of the diffused DQW and the corresponding diffused single QW cross over when $t\geqslant180$ s, as in Fig. 6, i.e., the highest gain peak of the diffused DQW becomes lower than that of the diffused single QW. This is because the difference between the two transition energies of the diffused DQW (100 meV) and that of the corresponding diffused single QW (146 meV) are very large, so that the effect of the transition energy difference is not significant in this case. However, the optical matrix element of the transition with the lowest photon energy of diffused DQW is smaller than that of the corresponding diffused single QW when $t\geqslant180$ s, as in Fig. 7. Therefore, the gain peak of the diffused DQW is lower than that of the diffused single QW. It should be noted that the photon energy of the largest gain peak of the diffused DQW is always higher than that of the diffused single QW. It is because the transition energy of a symmetric DQW is higher than the single QW with thickness equal to the summation of the two wells and the separation barrier of the DQW.[24] Moreover, for the case of $t\geqslant180$ s, the DQW is diffused to such an extent that it effectively becomes a single well with the Al content higher than that of the diffused single QW, which contributes to a higher transition energy for the diffused DQW. Concerning the rate of radiative spontaneous recombination (τ) of DQW

TABLE I. The gain peak and τ of $In_{0.53}Ga_{0.47}As/In_{0.52}Al_{0.48}As$ DQWs with an injected carrier density of $5\times10^{12}\,cm^{-2}$.

DQW structure (Å)	Peak gain (cm^{-1})	Peak τ $\times10^{14}$ (s^{-1})	DQW structure (Å)	Peak gain (cm^{-1})	Peak τ $\times10^{14}$ (s^{-1})
50/20/50	4797	1.575	50/10/50	4378	1.481
60/20/40	3800	1.357	50/20/50	4797	1.575
70/20/30	3220	1.010	50/30/50	4860	1.577
80/20/20	3373	1.071	50/40/50	4885	1.583
90/20/10	3396	1.072	50/50/50	4875	1.580

and the corresponding single QW, the maximum value of τ of diffused DQW is larger than that of the diffused single QW when $t<100$ s, as in Fig. 6. However, when $t>180$ s, τ of the diffused DQW becomes smaller. These variations are similar to that of the gain spectra of the two QW structures with fully inverted carrier population.

To maximize the material gain asymmetric $In_{0.53}(Al_aGa_{1-a})_{0.47}As/In_{0.52}Al_{0.48}As$ DQWs, with $n=5\times10^{12}\,cm^{-2}$ lattice matched to InP substrate, are addressed. By tailoring $In_{0.53}Ga_{0.47}As/In_{0.52}Al_{0.48}As$ DQW from a symmetric DQW structure of 50 Å/20 Å/50 Å which denotes the thickness of the left-hand side well, separation barrier, and right-hand side well to asymmetric DQWs of 60 Å/20 Å/40 Å, 70 Å/20 Å/30 Å, 80 Å/20 Å/20 Å, and 90 Å/20 Å/10 Å. The highest gain peak and τ generally decrease as compared to the symmetric DQW one as shown in Table I. It is because the energy difference between $C1S-HH1S$ and $C1A-HH1A$ significantly increases from the symmetric DQW (20 meV) to other asymmetric DQW. For instance, the energy difference of 90 Å/20 Å/10 Å DQW is 191 meV. To consider the composition effect of $In_{0.53}(Al_aGa_{1-a})_{0.47}As/In_{0.52}Al_{0.48}As$ DQW, the Al content in wells of 50 Å/20 Å/50 Å DQW is adjusted. The gain peak and τ decrease when Al content increases. When Al content increases from 0 to 0.2, the gain peak decreases from 4797 to 3000 cm^{-1} and the peak τ decreases from 1.575×10^{14} to $1.272\times10^{14}\,s^{-1}$ because both electron and hole quasi-Fermi levels decrease from 0.1476 eV (electron) and -3.28×10^{-3} eV (hole) to 0.1006 eV (electron) and -8.05×10^{-3} eV (hole), respectively. As a result, a symmetric DQW with no Al content in wells can provide the highest gain peak and τ. The effect of the separation-barrier thickness is studied by using symmetric $In_{0.53}Ga_{0.47}As/In_{0.52}Al_{0.48}As$ DQWs with different thicknesses of separation barrier. The gain peak and τ enhance when the barrier thickness widens from 10 to 30 Å and then saturate for a wider barrier thickness as shown in Table I. The enhancement is due to the reduction of the separation between $C1S-HH1S$ and $C1A-HH1A$. For instance, when the barrier thickness increases from 10 to 30 Å, the separation decreases from 57.9 to 7.3 meV. As a result, the optimized structure is $In_{0.53}Ga_{0.47}As/In_{0.52}Al_{0.48}As$ 50 Å/40 Å/50 Å DQWs. With interdiffusion, the gain peak generally decreases when t increases as the cases of 50 Å/50 Å/50 Å and 50 Å/20 Å/50 Å DQWs shown in Table II and Fig. 4, respectively. A similar trend can also be obtained for τ as the case of 50 Å/50 Å/50 Å shown in Table II. The main reason is due to the increase in separation between $C1S-HH1S$ and $C1A-HH1A$ as discussed previously. Consequently, symmetric $In_{0.53}Ga_{0.47}As/In_{0.52}Al_{0.48}As$ DQW can provide high material gain and τ. For the symmetric DQW with 50 Å wells, the separation barrier with thickness of ~40 Å can provide the highest gain peak and τ. With interdiffusion, the material gain peak and τ will generally decrease. It is also observed that a QW structure with a high material gain has a high radiative recombination rate.

Although interdiffusion will modify the refractive index of the DQW structure in the active region of optical devices, it will not significantly affect the waveguide properties and optical field profile. It is because in a typical optimized laser structure with five QWs as the active region, the optical confinement factor per well is only 0.0075.[25] Besides, the interdiffusion for tailoring the optical properties of the active region in a laser is weak[26] as compared to that for developing waveguides.[27] Therefore the change of refractive index in the active region due to interdiffusion should not significantly modify the guiding properties of the lasers structure. Besides, the increase of the separation barrier from 20 to 50 Å will not remarkably affect the optical confinement. For instance, there is a laser structure consisted five periods of DQW; each separated by a 150 Å barrier, sandwiched between two 1 μm $In_{0.52}Al_{0.48}As$ cladding layers. For the case the DQW at 50 Å/20 Å/50 Å, the optical confinement in the wells of the five DQW periods is ~0.1391, while that of the five-period 50 Å/50 Å/50 Å DQW laser structure is ~0.1356, i.e., the difference of the optical confinement is <3%.

B. Effects of injected carriers

When the injected carrier density (n) increases, the excitonic absorption of the diffused DQW with $t=7$ s is suppressed, as in Fig. 8(a). The exciton peak can no longer be resolved when n is increased to $5\times10^{10}\,cm^{-2}$. When n is further increased to $5\times10^{12}\,cm^{-2}$, the material gain with a

TABLE II. The gain peak and τ of 50 Å/50 Å /50 Å $In_{0.53}Ga_{0.47}As/In_{0.52}Al_{0.48}As$ diffused DQWs with an injected carrier density of $5\times10^{12}\,cm^{-2}$.

t (s)	Peak gain (cm^{-1})	Peak $\tau\times10^{14}$ (s^{-1})
0	4875	1.580
18	4618	1.509
36	4317	1.433
180	2279	1.069
360	854	0.845

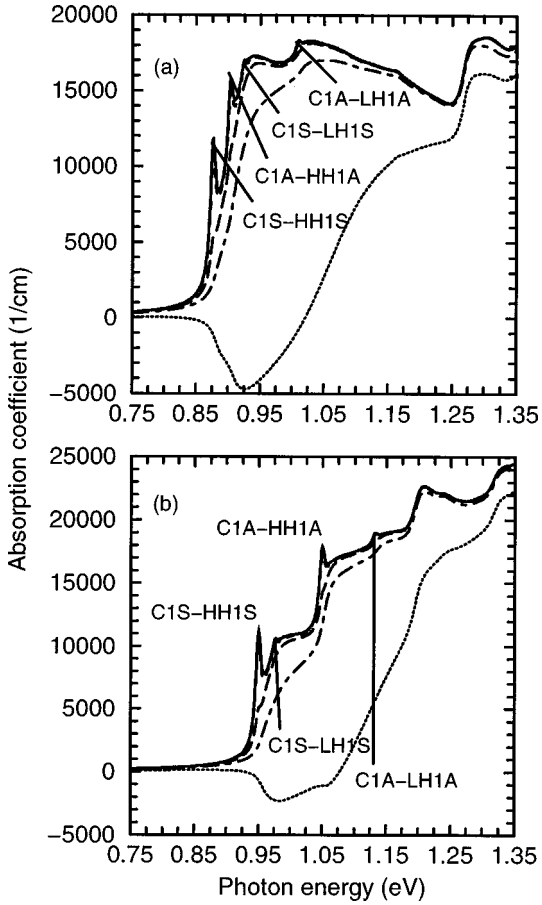

FIG. 8. TE absorption spectra of the diffused DQW; carrier density=$5\times10^{9}\,\mathrm{cm}^{-2}$ (solid line), $1\times10^{10}\,\mathrm{cm}^{-2}$ (dashed line), $5\times10^{10}\,\mathrm{cm}^{-2}$ (long-dashed line), $5\times10^{11}\,\mathrm{cm}^{-2}$ (dashed–dotted line), and $5\times10^{12}\,\mathrm{cm}^{-2}$ (dotted line): (a) annealing time $t=7$ s, (b) $t=180$ s.

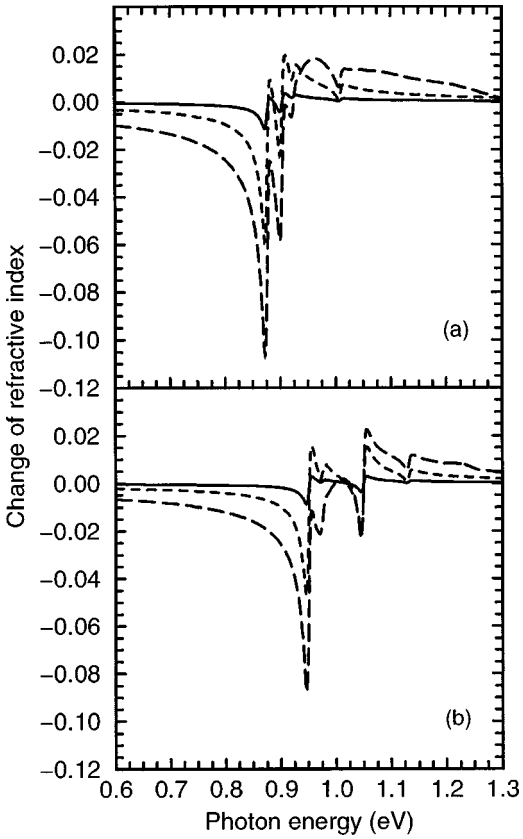

FIG. 9. TE refractive index change of the diffused DQW; carrier density=$1\times10^{10}\,\mathrm{cm}^{-2}$ (solid line), $5\times10^{10}\,\mathrm{cm}^{-2}$ (dashed line) and $5\times10^{11}\,\mathrm{cm}^{-2}$ (long-dashed line): (a) $t=7$ s, (b) $t=180$ s.

peak of $\sim4500\ \mathrm{cm}^{-1}$ is obtained at the photon energy of ~0.913 eV. At $t=180$ s, the features of the absorption spectrum of a typical single QW can be obtained from the diffused DQW, as in Fig. 8(b). The exciton peaks with photon energy in ascending order correspond to $C1S-\mathrm{HH}1S$, $C1S-\mathrm{LH}1S$, $C1A-\mathrm{HH}1A$, and $C1A-\mathrm{LH}1A$ for the diffused DQW with $t=180$ s, while that of the strongly coupled diffused DQW with $t=7$ s are $C1S-\mathrm{HH}1S$, $C1A-\mathrm{HH}1A$, $C1S-\mathrm{LH}1S$, and $C1A-\mathrm{LH}1A$. Moreover, an obvious ''step'' feature is obtained in the absorption spectrum of the 180 s annealed DQW because it effectively becomes a single QW, as in Fig. 2(a).

The change of n will modify the absorption coefficient and vary the refractive index, as in Fig. 9. The change of refractive index will be enhanced by increasing n. However, when t increases from 7 to 180 s, the change of refractive index decreases because the change of absorption coefficient decreases, as in Fig. 8. In addition, the fluctuating region of the refractive index spectra, with peaks and troughs corresponding to the interband transitions, is between 0.85 and 1.025 eV when $t=7$ s. This fluctuating region will shift to higher photon energies and become broader with an energy range from 0.915 to 1.15 eV when $t=180$ s. This is because the transitions are blueshifted and the subbands at $k_{\|}=0$ are separated out with increasing t, as in Fig. 2(b).

C. Effects of applied electric fields

As shown in Fig. 10(a), the energy difference between HH1S and HH1A increases when the applied field F increases. When $F=0$, the energy difference of the diffused DQW with $t=18$ s is smaller than that of the diffused DQW with $t=180$ s. However, the energy difference of the 18 s annealed DQW increases substantially with applied electric fields. For $F\geqslant25$ kV/cm, the energy difference of the 18 s annealed DQW becomes greater than that of the 180 s annealed DQW. Generally, when F increases, the spin splitting of the valence band due to the breaking of inversion symmetry is enhanced. However, the increase in the spin splitting with the applied electric field weakens with increasing t, as in Fig. 10(b). Consequently, the effects of applied electric fields on the diffused DQW subbands, including the increase in the energy difference between HH1S and HH1A and the increase in the spin splitting of the valence subbands, diminish when t increases.

With applied electric fields, the absorption spectra of the diffused DQWs with $n=5\times10^{9}\,\mathrm{cm}^{-2}$ are modified, due to the quantum confined Stark effect, as in Fig. 11. One of the interesting features of the strongly coupled diffused DQW with $t=18$ s is the establishment of the $C1S-\mathrm{HH}1A$ and $C1A-\mathrm{HH}1S$ excitonic absorption peaks. The former peak is blueshifted and the latter is redshifted when F increases. Up to $F=75$ kV/cm, they merge, as in Fig. 11(a), and thus the absorption coefficient increases to the highest peak. These

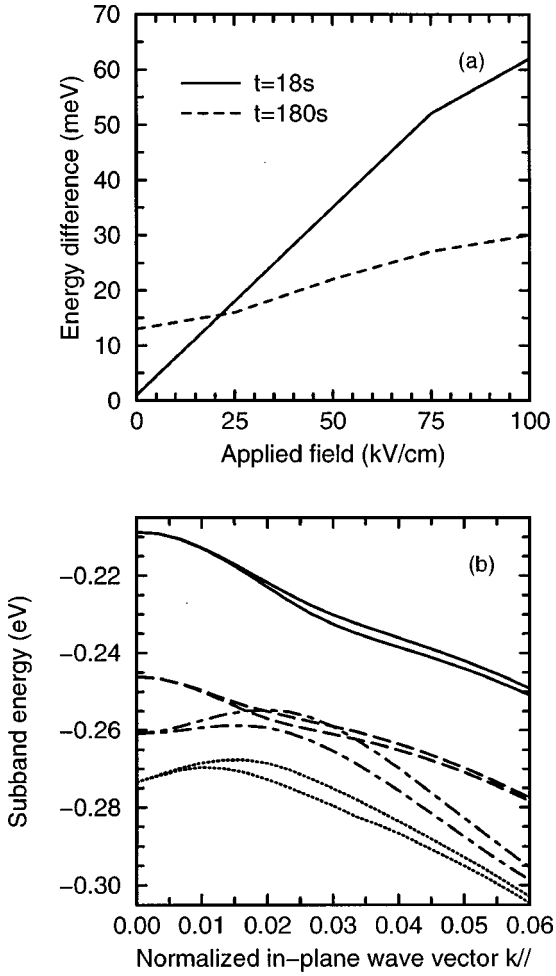

FIG. 10. (a) The energy difference between HH1*S* and HH1*A* of the diffused DQW at applied electric fields and annealing time of $t=18$ s (solid line), 180 s (dashed line). (b) HH1*S* and HH1*A* subbands at $F=75$ kV/cm; annealing time $t=18$ sHH1*S* (solid line), $t=18$ sHH1*A* (dashed–dotted line), $t=180$ sHH1*S* (long-dashed line), $t=180$ sHH1*A* (dotted line).

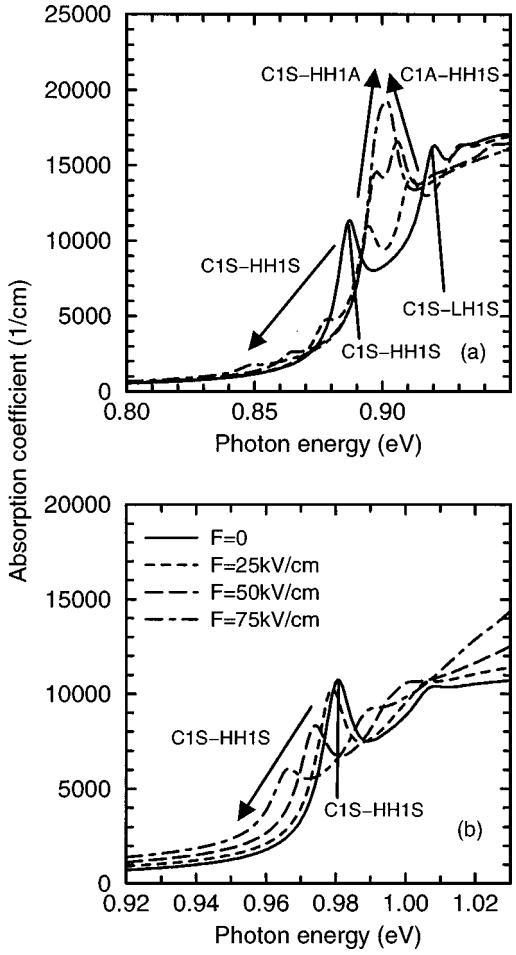

FIG. 11. TE absorption spectra of the diffused DQW with carrier density$=5\times10^{9}$ cm^{-2}. (a) annealing time $t=18$ s and (b) $t=360$ s;$F=0$ (solid line), 25 kV/cm (dashed line), 50 kV/cm (long-dashed line), 75 kV/cm (dashed–dotted line).

trends, i.e., $C1S-$HH1A and $C1A-$HH1S transitions moving closer together and the increase in absorption coefficient, are in good agreement with the experimental results of a strongly coupled DQW.[28] For the variation of other transitions, such as the blueshift of $C1A-$LH1A and redshift of $C1S-$HH1S, the observations depend on the exciton broadening factors used in the modeling, the quality of the DQW structures, and the experimental measurement techniques. Consequently, since the $C1S-$HH1S excitonic absorption peak is relatively weak for $F\geqslant 70$ kV/cm, as compared with the enhanced $C1S-$HH1A and $C1A-$HH1S exciton absorption peaks, the $C1A-$HH1S peak can be considered as the ''effective'' strong exciton absorption peak with the lowest transition energy. In this way, we can obtain a blueshift of the effective absorption peak from $F=0$ ($C1S-$HH1S at 0.887 eV) to $F=75$ kV/cm ($C1A-$HH1S at 0.906 eV) with a shift of 19 meV. When $t=360$ s, as the DQW is diffused to become a single graded QW, the features of the absorption spectra due to applied fields are similar to those of a typical single QW structure, as in Fig. 11(b). The strongest exciton peak is $C1S-$HH1S at $F=0$ for the 360 s annealed DQW instead of $C1S-$HH1A and $C1A-$HH1S excitonic absorption peaks at $F\neq 0$ for the 18 s annealed DQW. Moreover, the $C1S-$HH1S absorption peak for the 360 s annealed DQW at $F=75$ kV/cm is moderately higher than that of the 18 s annealed DQW. The absorption change of 3600 cm^{-1} can be obtained although the loss is large (2200 cm^{-1}). It should be noted that in order to obtain a large absorption change or refractive index change for use in optical modulators, asymmetric DQW should be used,[8,9] although the optimization of asymmetric DQW for optical modulators is not the subject of the work presented here.

When n increases to 5×10^{12} cm^{-2}, carrier screening effects become important, especially with applied electric fields, as in Fig. 12(a). At $F=0$, the potential profile of the 18 s annealed DQW with screening effects is close to that of the diffused DQW without screening. Also, the envelope functions with and without screening are similar to each other. Therefore, the gain spectra with and without screening effects overlap and cannot be distinguished, as in Fig. 12(b). When F increases to 75 kV/cm, the screening effects will weaken the tilting of the diffused DQW due to the applied electric field. Without screening, the envelope function dominantly distributes in the right-hand side quantum well.

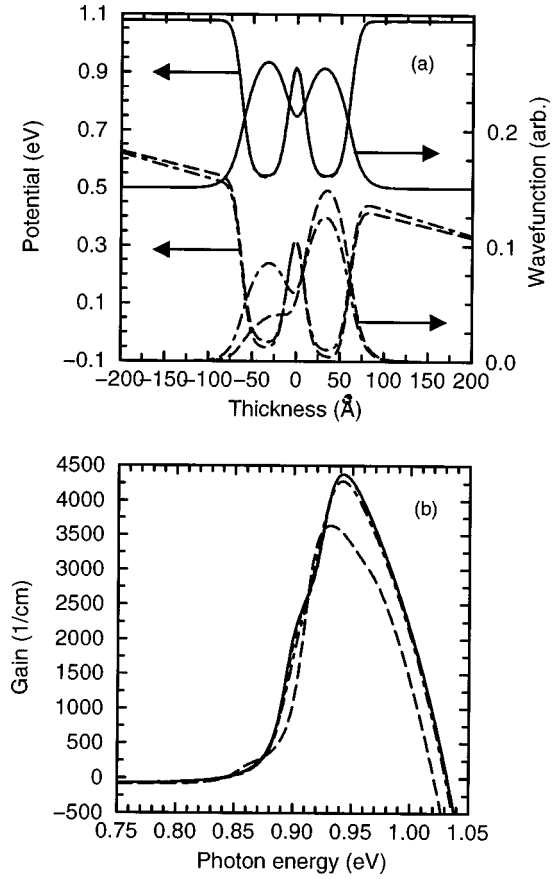

FIG. 12. (a) The conduction-band potential profile and $C1S$ envelope function and (b) the TE gain spectra of the diffused DQW with $t=18$ s; $F=0$ without screening (solid line), $F=0$ with screening (dashed line), $F=75$ kV/cm without screening (long-dashed line), and $F=75$ kV/cm with screening (dashed–dotted line).

However, with screening, because of the flattening of the potential profile, the envelope function in the left-hand side quantum well recovers. As a result, at $F=75$ kV/cm, the material gain of the diffused DQW with screening effects is enhanced and blueshifted as compared to that without screening, as in Fig. 12(b). Consequently, the gain switching of the diffused DQW due to a reverse bias will be reduced by screening effects.

IV. CONCLUSIONS

In this article, the subband structures and optical properties of $In_{0.53}(Al_aGa_{1-a})_{0.47}As/In_{0.52}Al_{0.48}As$ DQW have been theoretically investigated with interdiffusion. The results show that, with suitable annealing time, the DQW is diffused to become a single graded QW. Therefore, the characteristic features in the interband transitions and the optical properties of a strongly coupled DQW can be obtained in a short-time diffused DQW, while that of a typical single QW can be provided by a long-time diffused DQW.

In optimizing the DQW structure, results show that symmetric DQWs with no Al content in wells can provide high material gain and radiative spontaneous recombination rate. For the symmetric $In_{0.53}Ga_{0.47}As/In_{0.52}Al_{0.48}As$ DQW with 50 Å wells, the largest gain peak and τ can be achieved by using a 40 Å separation barrier. With interdiffusion, the material gain and τ will decrease but the reduction will saturate when the symmetric DQW is diffused to become a single QW structure. The reduction is primarily due to the enhancement of the separation between the $C1S-HH1S$ and $C1A-HH1A$ transitions. By subjecting the 50 Å/20 Å/50 Å $In_{0.53}Ga_{0.47}As/In_{0.52}Al_{0.48}As$ DQW and an as-grown single QW with a well width of 120 Å to the same annealing conditions, we find that for a short annealing time the diffused DQW can provide a larger material gain and τ than the corresponding diffused single QW for use in lasers. The photon energy associated with the largest gain peak of the diffused double QW is always higher than that of the diffused single QW. Moreover, since Al diffuses into the wells, the transition energy increases so that the operating wavelength of the DQW structure can be tailored.

When the applied electric field increases, the enhancement of the separation between HH1S and HH1A subbands of a slightly diffused DQW is faster than that of the extensively diffused DQW. In addition, the spin splitting of the valence subbands of the diffused DQW, due to applied electric fields, will weaken with increasing annealing time. These results are mainly due to the reduction of the coupling between the two wells as the annealing time increases.

ACKNOWLEDGMENT

This work was supported by the Croucher Foundation and the National Research Council of Canada.

[1] T. Miyazawa, Y. Kawamura, and O. Mikami, Jpn. J. Appl. Phys., Part 2 **27**, L1731 (1988).
[2] R. J. Baird, T. J. Potter, G. P. Kothiyal, and P. K. Bhattacharya, Appl. Phys. Lett. **52**, 2055 (1988).
[3] J. Y. Chi, E. S. Koteles, and R. P. Hoimstrom, Appl. Phys. Lett. **53**, 2185 (1988).
[4] S. O'Brien, J. R. Shealy, V. K. F. Chia, and J. Y. Chi, J. Appl. Phys. **69**, 5256 (1990).
[5] T. Miyazawa, Y. Suzuki, Y. Kawamura, H. Asai, and O. Mikami, Jpn. J. Appl. Phys., Part 2 **28**, L730 (1989).
[6] K. S. Seo, P. K. Bhattacharya, G. P. Kothlyal, and S. Hong, Appl. Phys. Lett. **49**, 966 (1986).
[7] P. K. Gug and W. E. Hagston, Appl. Phys. Lett. **73**, 1547 (1998).
[8] W. C. H. Choy, E. H. Li, and B. L. Weiss, IEEE J. Quantum Electron. **34**, 1846 (1998).
[9] K. W. Gossen, J. E. Cunningham, and W. Y. Jan, Appl. Phys. Lett. **64**, 1071 (1994).
[10] D. Ahn and T. K. Yoo, Jpn. J. Appl. Phys., Part 1 **31**, 1055 (1992).
[11] N. Susa, IEEE J. Quantum Electron. **31**, 92 (1995).
[12] Y. Chan, W. C. Shiu, W. K. Tsui, and E. H. Li, Mater. Res. Soc. Symp. Proc. **450**, 337 (1997).
[13] J. M. Luttinger and W. Kohn, Phys. Rev. **97**, 869 (1995).
[14] H. Asai and K. Oe, J. Appl. Phys. **54**, 2052 (1983); R. People, Phys. Rev. **32**, 1405 (1995).
[15] P. Lawaetz, Phys. Rev. B **4**, 3460 (1971).
[16] D. Ahn and S. L. Chuang, J. Appl. Phys. **64**, 6143 (1988).
[17] W. C. H. Choy, E. H. Li, M. C. Y. Chan, and B. L. Weiss, IEEE J. Quantum Electron. **34**, 913 (1998).
[18] G. Bastard and J. A. Brum, IEEE J. Quantum Electron. **22**, 1625 (1986).
[19] D. J. BenDaniel and C. B. Duke, Phys. Rev. **152**, 683 (1966).
[20] I. Galbraith and G. Duggan, Phys. Rev. B **40**, 5515 (1989).
[21] W. C. H. Choy, Ph.D. thesis, University of Surrey, Guildford, Surrey, UK, 1998.
[22] D. S. Chemla, D. A. B. Miller, P. W. Smith, A. C. Gossard, and W. Wiegmann, IEEE J. Quantum Electron. **20**, 265 (1994).
[23] W. C. H. Choy, P. J. Hughes, B. L. Weiss, E. H. Li, K. Hong, and

D.Pavlidis, Appl. Phys. Lett. **72**, 338 (1998).
[24] D. Atkinson, G. Parry, and E. J. Austin, Semicond. Sci. Technol. **5**, 516 (1990).
[25] P. W. A. McIroy, A. Kurobe, and Y. Uematsu, IEEE J. Quantum Electron. **12**, 1958 (1985).
[26] P. J. Poole, S. Charbonneau, M. Dion, G. C. Aers, M. Buchannan, R. D. Goldberg, and I. V. Mitchell, IEEE Photonics Technol. Lett. **8**, 16 (1996).
[27] J. E. Haysom, A. Delage, J. J. He, E. S. Koteles, P. J. Poole, Y. Feng, R. D. Goldberg, I. V. Mitchell, and S. Charbonneau, IEEE J. Quantum Electron. **35**, 1354 (1999).
[28] N. Debbar, S. Hong, J. Singh, P. Bhattacharya, and R. Sahai, J. Appl. Phys. **65**, 383 (1989).